Single crystal elasticity of majoritic garnets: Stagnant slabs and thermal anomalies at the base of the transition zone

Martha G. Pamato [a,*,1], Alexander Kurnosov [a], Tiziana Boffa Ballaran [a], Daniel J. Frost [a], Luca Ziberna [a,2], Mattia Giannini [a,3], Sergio Speziale [b], Sergey N. Tkachev [c], Kirill K. Zhuravlev [c], Vitali B. Prakapenka [c]

[a] *Bayerisches Geoinstitut, Universitaet Bayreuth, D-95440 Bayreuth, Germany*
[b] *Deutsches GeoForschungsZentrum GFZ, Telegrafenberg, 14473 Potsdam, Germany*
[c] *GSECARS, University of Chicago, 60637 Chicago, IL, USA*

ARTICLE INFO

ABSTRACT

The elastic properties of two single crystals of majoritic garnet ($Mg_{3.24}Al_{1.53}Si_{3.23}O_{12}$ and $Mg_{3.01}Fe_{0.17}Al_{1.68}Si_{3.15}O_{12}$), have been measured using simultaneously single-crystal X-ray diffraction and Brillouin spectroscopy in an externally heated diamond anvil cell with Ne as pressure transmitting medium at conditions up to ~30 GPa and ~600 K. This combination of techniques makes it possible to use the bulk modulus and unit-cell volume at each condition to calculate the absolute pressure, independently of secondary pressure calibrants.

Substitution of the majorite component into pyrope garnet lowers both the bulk (K_s) and shear modulus (G). The substitution of Fe was found to cause a small but resolvable increase in K_s that was accompanied by a decrease in $\partial K_s/\partial P$, the first pressure derivative of the bulk modulus. Fe substitution had no influence on either the shear modulus or its pressure derivative. The obtained elasticity data were used to derive a thermo-elastic model to describe V_s and V_p of complex garnet solid solutions. Using further elasticity data from the literature and thermodynamic models for mantle phase relations, velocities for mafic, harzburgitic and lherzolitic bulk compositions at the base of Earth's transition zone were calculated. The results show that V_s predicted by seismic reference models are faster than those calculated for all three types of lithologies along a typical mantle adiabat within the bottom 150 km of the transition zone. The anomalously fast seismic shear velocities might be explained if laterally extensive sections of subducted harzburgite-rich slabs pile up at the base of the transition zone and lower average mantle temperatures within this depth range.

1. Introduction

Seismic velocity profiles of the Earth's interior provide essential information for constraining the thermal and chemical state of the mantle (Anderson and Bass, 1986; Irifune and Ringwood, 1987a; Ita and Stixrude, 1992). The correct interpretation of these profiles in terms of mantle mineralogy and chemistry, however, re-quires laboratory or computational data on the elasticity of candidate minerals at conditions of the Earth's mantle. In this context, knowledge of the thermo-elastic properties of garnet solid solutions are essential, since they make up a major proportion of both mafic and ultramafic rocks in the upper mantle and transition zone (Irifune and Ringwood, 1987a). Garnets recovered from the Earth's mantle crystallize in the cubic space group $Ia\bar{3}d$ forming a series of complex solid solutions that are described using the crystal-structural formula $^{VIII}X_3{}^{VI}Y_2{}^{IV}Z_3O_{12}$. Large cations, X = Mg, Ca, Fe^{2+}, occupy the 8-fold coordinated dodecahedral sites, medium sized cations, Y = Al, Fe^{3+}, Cr, occupy the octahedral sites, whereas the tetrahedral Z site is occupied by Si. At pressures above 5 GPa the coupled substitution of Si and Mg (and Fe) onto the Y site occurs in garnets within mantle assemblages as a result of the break-down of both orthopyroxene and clinopyroxene. This, so called, majorite substitution increases the proportion of garnet in man-

---

Table 1
Starting materials in wt.% of oxides.

	Pyrope glass	Mixture Py1	Mixture Py3	Enstatite glass	Fe-majorite	Mixtures A′, B′, C′, D′
Al_2O_3	25.29	19.95	22.3	–	12.91	A′: 50% enstatite glass – 50% mixture Py1 (10.56 wt.% H_2O)
MgO	44.71	23.66	26.45	40.15	26.96	B′: 50% enstatite glass – 50% mixture Py2 (7.92 wt.% H_2O)
SiO_2	29.99	35.27	39.43	59.85	42.8	C′: 50% enstatite glass – 50% mixture Py3 (5.91 wt.% H_2O)
Fe_2O_3	–	–	–	–	5.28	D′: 50% enstatite glass – 50% mixture Py4 (1.48 wt.% H_2O)
H_2O	–	21.12	11.81	–	12.04	
Sum	100	100	100	100	99.99	

Note: mixture Py2 = 25% pyrope glass + 75% mixture Py1; mixture Py4 = 75% pyrope glass + 25% mixture Py3.

tle rocks at the expense of pyroxenes in the Earth's deep upper mantle and transition zone (Ringwood, 1967). The Al-free garnet end-member is referred to as majorite, Mj ($Mg_4Si_4O_{12}$) and crystallizes with tetragonal symmetry due to ordering of Mg and Si on the octahedral sites. Pure Mj is stable at pressures between 16 and 23 GPa and temperatures above 1600 °C (Kato and Kumazawa, 1985; Angel et al., 1989). In upper mantle ultramafic rocks garnets are solid solutions that are dominated by the end member pyrope (Py, $Mg_3Al_2Si_3O_{12}$) but have sub-equal proportions of almandine (Alm, $Fe_3Al_2Si_3O_{12}$) and grossular (Gr, $Ca_3Al_2Si_3O_{12}$). With increasing pressure, however, the Mj end member becomes increasingly important and dominates in the transition zone (410–660 km depth). A key issue concerning the structure of the Earth's interior is the extent and scale at which the mantle can be considered homogeneous. A number of studies have proposed, for example, that the mantle may become richer in mafic material with depth (e.g. Anderson and Bass, 1986). One of the main expressions of such chemical heterogeneity in the mantle would be variation in the chemistry and proportion of garnet. Garnets constitute approximately 40% by volume of ultramafic compositions and 70% of mafic compositions (Anderson and Bass, 1986; Irifune and Ringwood, 1987a; Ita and Stixrude, 1992), but garnets formed from mafic assemblages will have greater Gr and Alm contents and in the transition zone less Mj compared to ultramafic assemblages. Knowledge of how the elastic properties of garnet change as the bulk chemistry changes is, therefore, important.

Several studies have investigated the elastic properties of Py–Mj garnets at room pressure and temperature (Bass and Kanzaki, 1990; O'Neill et al., 1991). Moreover elastic moduli measurements have also been performed at high pressure and room temperature, using ultrasonic techniques on polycrystalline aggregates (Rigden et al., 1994; Gwanmesia et al., 1998; Chen et al., 1999; Wang and Ji, 2001) and through the use of Brillouin spectroscopy on both single crystals (Conrad et al., 1999; Sinogeikin and Bass, 2000; Murakami et al., 2008) and powdered samples (Sinogeikin and Bass, 2002). Recent improvements in ultrasonic techniques coupled with synchrotron X-ray radiation have allowed sound velocity measurements on polycrystalline samples along the Py–Mj solid solution to be performed at simultaneous high P and T (Irifune et al., 2008; Gwanmesia et al., 2009; Liu et al., 2015). Furthermore the single-crystal elasticity of an iron-bearing pyrope was recently obtained simultaneously at high-pressures (up to 20 GPa) and high-temperature (750 K) using Brillouin spectroscopy and X-ray diffraction (Lu et al., 2013). While the value of the bulk and shear moduli, K_s and G, reported by these studies cover a relatively small range, the exact dependence particularly of K_s on Mj content is unclear, large discrepancies in elastic moduli pressure derivatives exist, the thermal properties are poorly constrained as is the effect of the Alm content. Consequently, the interpretations of seismic velocity gradients in the transition zone remain uncertain.

The aim of this study is, therefore, to constrain the elastic properties of majoritic garnets as a function of density, temperature and composition under hydrostatic conditions by employing a combination of single-crystal Brillouin scattering and X-ray diffraction

measurements. The simultaneous measurement of elastic properties and density are used to also obtain absolute values of the experimental pressure, avoiding in this way any systematic errors that may be introduced through the use of secondary pressure calibrations. The elasticity data obtained are fitted to a self-consistent thermo-elastic model from which thermodynamic properties of the garnet end-members are estimated. Acoustic velocities of mafic, harzburgitic and lherzolitic assemblages are then calculated along a typical mantle adiabat at conditions of the Earth's transition zone by combining our garnet model with properties for coexisting minerals from the literature. The results are then compared with seismic reference models reported over the same depth interval to constrain the plausible mineralogy and temperature at the base of the Earth's transition zone.

2. Experimental methods

2.1. Sample synthesis and characterization

The growth of large crystals is usually facilitated by adding a flux to the starting material, such as H_2O, in order to lower the melting temperature and allow larger crystals to grow from the surrounding melt. The flux to starting material ratio is an important factor in determining the size of the final crystals. In order to assess the optimal H_2O content for the growth of large single crystals, four different majoritic garnet starting mixtures were prepared by mixing in a 50/50 proportion an enstatite glass and four pyrope mixtures (Py1, Py2, Py3 and Py4) with different H_2O contents (Table 1).

The four pyrope mixtures were then mixed with the enstatite glass to produce hydrous majoritic garnet starting mixtures with differing H_2O contents, A′, B′, C′, D′ (Table 1). These were loaded into a multi-chamber capsule fabricated from a 2 mm diameter rhenium rod.

High-pressure experiments aimed at producing majoritic garnets were carried out using a 5000 t multi-anvil apparatus at the Bayerisches Geoinstitut. A 18 mm edge length Cr_2O_3-doped (5 wt.%) MgO octahedron was used as a pressure medium with tungsten carbide cubes of 52 mm edge length and 11 mm truncation edge length (18/11 assembly). The pressure calibrations for the assembly used in this study are reported in Keppler and Frost (2005). The samples were first pressurized to 17 GPa followed by heating at 1900 °C for 5 min. After heating at high pressure, the experiments were quenched by shutting off the power and the run-products were recovered after decompressing for 18 h. The recovered capsules were embedded in epoxy resin, ground and polished for electron probe microanalysis. Single-crystals of majoritic garnet (up to ~200 μm in length) were obtained from the starting composition (mixture A′) that contained the largest amount of water (Fig. S1, supplementary information).

An iron bearing majoritic garnet with a similar composition to that recovered above was also prepared from a glass starting material that contained H_2O added as $Mg(OH)_2$ (Fe-majorite, see Table 1). An oxide mixture of Al_2O_3, SiO_2 and Fe_2O_3 was initially melted in air at 1600 °C for twenty minutes and then

rapidly quenched in icy water. This glass was then reduced in a 1-atmosphere furnace, at 1000 °C and at an oxygen fugacity (fO_2) of 2 logs units below the quartz–fayalite–magnetite oxygen buffer for approximately 12 h. This process was performed twice in order to ensure the complete reduction of the mixture. $Mg(OH)_2$ was then added to the glass to obtain a hydrous composition. The starting material was loaded into a double capsule consisting of a 1.6 mm diameter Re inner capsule and an outer capsule made of a 2 mm diameter platinum tube, welded closed at both ends. The synthesis run was performed using the same procedure and conditions followed for the iron-free samples.

Element concentrations in the recovered samples were measured with a JEOL JXA-8200 electron probe microanalyser (EPMA), operating at 15 kV and 15 nA. The electron beam size was approximately 1–2 μm in diameter and the peak counting times were 20 s. Enstatite or diopside, spinel, forsterite, and metallic iron were used as standards for determining the concentrations of Si, Al, Mg and Fe respectively. The chemical analysis resulted in the following composition: 32.0 (6)% MgO, 47.5 (9)% SiO_2, 19 (2)% Al_2O_3 (in wt.), for the Py–Mj garnet (hereafter named $Py_{76}Mj_{24}$) and 29.5(5)% MgO, 46(1)% SiO_2, 3.3(5)% FeO, 21(2)% Al_2O_3 (in wt.) for the iron bearing sample (hereafter named $Py_{78}Alm_6Mj_{16}$). The chemical formulas are $Mg_{3.24}Al_{1.53}Si_{3.23}O_{12}$ and $Mg_{3.01}Fe_{0.17}Al_{1.68}Si_{3.15}O_{12}$, respectively.

FTIR analyses were performed on crystals of $Py_{76}Mj_{24}$ produced in the same experiment and show OH absorption bands consistent with approximately 20 ppm wt. H_2O. Measurements were carried out at the Laboratoire Magmas et Volcans (LMV) in Clermont-Ferrand, France. The quantitative analyses were performed following the calibration of Paterson (1982). The synthesized majoritic garnets can, therefore, be considered to contain negligible amounts of H_2O.

2.2. Simultaneous X-ray diffraction and Brillouin scattering

The P–V–T equations of state and the compressional, V_p, and shear, V_s, sound velocities of two single-crystals of majoritic garnet ($Py_{76}Mj_{24}$ and $Py_{78}Alm_6Mj_{16}$) were each determined by means of simultaneous Brillouin spectroscopy and X-ray diffraction. High quality single-crystals, of ~70 μm in size, were selected based on their sharp diffraction profiles. The crystals were parallel polished into platelets with a thickness of 10–18 μm and then loaded into piston cylinder diamond anvil cells. Boehler–Almax diamonds were employed with 400–350 μm culets in combination with tungsten carbide seats. Rhenium gaskets of 200 μm in thickness were pre-indented to 40–55 μm before drilling 250 μm cylindrical holes. Single-crystals of Sm:YAG (Sm-doped $YAlO_3$ garnet) as well as ruby chips were added as secondary pressure calibrants. A neon gas pressure medium was loaded into the sample chamber using the high pressure gas loading devices at the Bayerisches Geoinstitut (Kurnosov et al., 2008) as well as at GSECARS (Rivers et al., 2008).

The pressure inside the cell was monitored before and after each Brillouin and X-ray measurement using an Acton standard series spectrograph from Princeton Instruments, employing the same laser and the same geometry as in the Brillouin experiment. An external resistive heater suitable for the piston cylinder type cells employed in this study was designed and placed around the diamonds for achieving high temperatures (see text S1 supplementary information). An S-type thermocouple located near the diamond surface was used to monitor the temperature inside the cell. However, to constrain the temperature inside the high pressure chamber without relying uniquely on the thermocouple, an alternative approach was used. The fluorescence shifts of Sm:YAG, which are independent of temperature, were used to determine pressure (Trots et al., 2013), whereas temperature was determined using the fluorescence of ruby (Rekhi et al., 1999) by fixing the

pressure value obtained from the Sm:YAG measurement. Maximum temperatures reached estimated in this way were 558 K and 470 K for $Py_{76}Mj_{24}$ and $Py_{78}Alm_6Mj_{16}$ respectively. However, the maximum thermocouple temperature readings were 600 K for $Py_{76}Mj_{24}$ and 650 K for $Py_{78}Alm_6Mj_{16}$, i.e. larger than the actual temperatures experienced by the majoritic samples.

Simultaneous acquisition of density and sound velocities at room pressure was performed at the Bayerisches Geoinstitut. The lattice parameters of both samples were determined using eight-position centering of 15 Bragg reflections ($25° < 2\theta < 40°$) according to the procedure of King and Finger (1979) on a Huber diffractometer equipped with point detector and driven by the program SINGLE (Angel and Finger, 2011). The resulting unit-cell volumes are 1506.6 (5) Å^3 and 1506.8 (1) Å^3 for $Py_{76}Mj_{24}$ and $Py_{78}Alm_6Mj_{16}$ respectively. The unit-cell volumes are practically identical because Alm replaces Mj in the second sample and both components have a qualitatively similar effect on the volume. Typical half-widths of the ω profiles of different reflections varied between 0.060° and 0.100°. Brillouin scattering measurements were performed in a 80° symmetric/platelet scattering geometry with plate spacing of 4 mm using a coherent Verdi V2 solid state Nd:YVO_4 frequency doubled laser ($\lambda = 532.0$ nm) at the power of ~150–200 mW. The room pressure Brillouin scattering measurements of $Py_{78}Alm_6Mj_{16}$ were performed at the GeoForschungsZentrum (GFZ) in Potsdam as well as at PETRA III in Hamburg, employing a 60 and 49° forward symmetric scattering geometry with plate spacing of 6 mm and 8 mm respectively. A coherent Verdi V2 solid state Nd:YVO_4 frequency doubled laser ($\lambda = 532.0$ nm) was used.

Simultaneous measurements of sound velocities and density at different pressures and temperatures were performed at the BM-13-D (GSECARS) beamline at the Advanced Photon Source (APS). The samples were each measured first upon compression up to approximately 20 and 21 GPa at room temperature and then heated to 558 K ($Py_{76}Mj_{24}$) and 470 K ($Py_{78}Alm_6Mj_{16}$) respectively. During heating the pressure increased to 30 GPa, therefore Brillouin spectra and density were measured along an isotherm (at high temperature) upon decompression. X-ray diffraction measurements were performed using a Perkin Elmer detector, collecting step scans in an omega range of 50° or 70° with a step size of 1° and 5 s/step exposure time. Brillouin scattering measurements were performed with a six-pass Sandercock-type tandem Fabry–Pérot interferometer using a coherent Verdi V2 solid state Nd:YVO_4 frequency doubled laser ($\lambda = 532.0$ nm) as a light source. Measurements were performed in a 50° symmetric/platelet scattering geometry with plate spacing of 6.5–7 mm. Brillouin spectra were collected with a laser power of 400 mW. Acoustic velocities, $V_{acoustic}$, were determined from the frequency shift using the following relationship (Whitfield et al., 1976):

$$V_{acoustic} = \Delta \nu * \lambda_0 / 2 * \sin(\theta / 2) \qquad (1)$$

where $\Delta \nu$ is the measured Brillouin shift, λ_0 is the incident laser wavelength, θ is the external scattering angle.

3. Results

3.1. Elasticity

The acoustic velocities of the $Py_{76}Mj_{24}$ and $Py_{78}Alm_6Mj_{16}$ samples measured at ambient conditions in different crystallographic directions as a function of χ angle are shown in Fig. 1.

Typical Brillouin spectra are also reported in the insets in the same Figure. The elastic anisotropy of the two majoritic-garnets is practically negligible both at ambient conditions and at high pressures and temperatures, as also observed for other

3
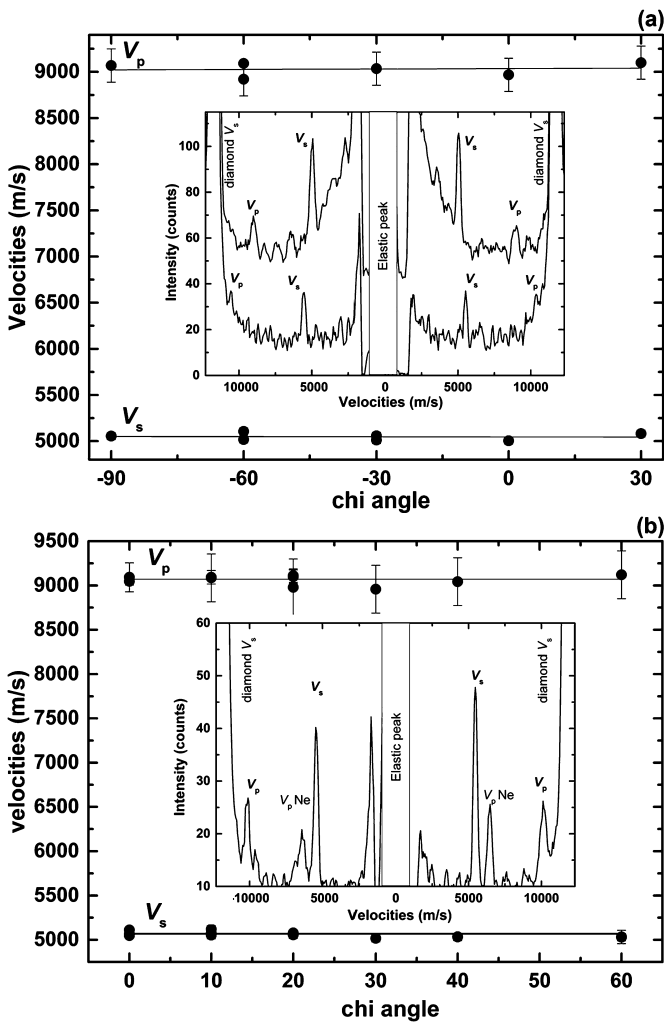
Fig. 1. (a) Compressional and shear wave velocities of $Py_{76}Mj_{24}$ as a function of crystallographic direction at room pressure and temperature. Inset: Brillouin spectra collected for a given crystallographic orientation at room pressure and temperature (top) and at 28.8 GPa and 558 K (bottom). (b) Compressional and shear wave velocities of $Py_{78}Alm_6Mj_{16}$ as a function of crystallographic direction at room pressure and temperature. The Brillouin spectrum reported in the inset was collected at 21.1 GPa.

garnets (e.g. Sinogeikin and Bass, 2000; Murakami et al., 2008; Lu et al., 2013).

The measured sound velocities are a function of the wave propagation direction and polarization q_i (referred to the crystal reference system), the elastic moduli C_{ijkl} and the density ρ of a given material, according to the Christoffel equation:

$$\left|C_{rlsm}q_lq_m - \rho V_{acoustic}^2\delta_{rs}\right| = 0 \tag{2}$$

where δ_{rs} is the Kronecker delta. Elastic constants can thus be obtained by fitting the solutions of the equation of motion to the measured sound velocities. However, as reported in previous studies (Murakami et al., 2008), the elastic constants of majoritic garnet can also be calculated by averaging the measured acoustic velocities over several non-symmetric directions given the negligible anisotropy. The aggregate values so obtained are indistinguishable, within experimental uncertainties, from those derived from least-squares fitting to Christoffel's equation. In this study, aggregate V_p and V_s wave velocities were obtained as the average of all longitudinal and transverse velocity measurements (for up to three orientations) at each pressure and temperature. The aggregate elastic moduli were then calculated from these aggregate velocities.

The majoritic single-crystal elastic moduli can then be related to the aggregate moduli through the following equations:

$$C_{11} = K_s + 4/3G = \rho V_P^2 \tag{3}$$
$$C_{44} = G = \rho V_S^2 \tag{4}$$
$$C_{12} = K_s - 2/3G = \rho\left(V_P^2 - 2V_S^2\right) \tag{5}$$

assuming the equality:

$$2C_{44} = C_{11} - C_{12} \tag{6}$$

The elastic properties and sound velocities of both samples as a function of density, pressure and temperature are summarized in Table 2.

Brillouin spectra collected on samples within diamond anvil cells at different pressures, temperatures and orientations typically have different signal to noise ratios that depend on the crystal optical quality and its orientation in addition to the laser focusing, sample alignment and collection time. The resolution of such spectra will influence the uncertainties on the V_s and V_p values used to obtain the elastic constants. The uncertainties on the velocities of the garnet crystals were assessed using a set of Brillouin spectra collected for the same sample but with different signal to noise ratios, varied by adjusting the length of data collection time between one hour to several days. A "calibration curve" was then constructed that describes the standard deviation on the velocity measurements as a function of the signal to noise ratio. Uncertainties of 20 m/s, i.e. 0.2–0.4% can be obtained when the best alignment is achieved, but usually they are larger than this value (see text S2 supplementary information).

3.2. Absolute pressure determination

An important advantage in making simultaneous measurements of density and sound velocities for the same sample at the same conditions it that it allows pressure to be determined without having to rely on a secondary pressure scale, such as that of the ruby fluorescence scale. For each experimental point, the absolute pressure (Table 2) was determined according to the equation

$$P = \int_{V_0}^{V} \frac{K_T(V)}{V}dV \tag{7}$$

where the unit-cell volume (V) was determined by means of X-ray diffraction, and the isothermal bulk modulus K_T was derived from the adiabatic bulk modulus K_S calculated using Brillouin sound velocities, according to the following expression:

$$K_s = K_T(1 + \alpha\gamma T) \tag{8}$$

where α is the volume thermal expansion and γ is the Grüneisen parameter. The values of α and γ for majoritic garnets were assumed to be equal to those of pyrope and were taken from Ahrens (1995).

The variation of the shear (V_S) and compressional (V_P) wave velocities as a function of absolute pressure obtained in this study at high pressures and temperatures are reported in Fig. 2.

The values of V_S and V_P wave velocities of $Py_{76}Mj_{24}$ and $Py_{78}Alm_6Mj_{16}$ are very similar at room pressure, however, they deviate at high pressures, with $Py_{76}Mj_{24}$ displaying faster velocities due to the higher pressure derivative of the elastic moduli.

3.3. Determination of P–V–T EoS of majoritic garnets

The high-pressure and temperature elastic properties of majoritic garnets are described using the self-consistent thermodynamic formalism described by Stixrude and Lithgow-Bertelloni (2005). This model employs a Mie–Grüneisen equation of state

Table 2

Single-crystal and aggregate elastic properties, aggregate sound velocities as a function of absolute pressure, temperature and density of majoritic garnets.

ρ (g/cm^3)	P_{abs} (GPa)	T (K)	C_{11} (GPa)	C_{12} (GPa)	C_{44} (GPa)	V_s (km/s)	V_p (km/s)	K_S (GPa)	G (GPa)
Py$_{76}$Mj$_{24}$									
3.552(3)	0.00010(1)	298	290(3)	109(2)	91(1)	5.05(1)	9.03(3)	169(3)	91(1)
3.692(3)	7.1(2)	298	333(6)	128(6)	102(1)	5.26(2)	9.50(8)	197(6)	102(1)
3.729(3)	9.10(11)	298	349(4)	139(3)	105(1)	5.30(2)	9.67(2)	209(3)	105(1)
3.750(3)	10.2(4)	298	351(8)	140(8)	106(1)	5.31(2)	9.68(10)	210(8)	106(1)
3.783(3)	12.2(7)	298			109(1)	5.37(2)			109(1)
3.844(3)	15.9(5)	298	390(4)	166(2)	112(1)	5.40(2)	10.080(8)	241(3)	112(1)
3.840(3)	15.6(7)	298	385(9)	161(9)	112(1)	5.41(5)	10.01(10)	235(9)	112(1)
3.892(3)	18.9(4)	298	406(4)	176(2)	115(1)	5.436(7)	10.22(2)	253(3)	115(1)
3.904(3)	19.7(9)	298	414(10)	180(9)	117(2)	5.47(2)	10.29(11)	258(9)	117(2)
4.024(4)	28.8(1.8)	558	463(14)	216(14)	123(3)	5.53(5)	10.72(15)	298(14)	123(3)
3.980(4)	25(2)	558	422(17)	185(17)	119(3)	5.46(4)	10.30(20)	264(14)	119(3)
3.926(4)	22.0(1.0)	558	409(9)	181(9)	114(2)	5.39(5)	10.21(10)	257(9)	114(2)
3.834(4)	16.2(5)	558	382(6)	160(6)	111(2)	5.38(3)	9.98(7)	234(6)	111(2)
Py$_{78}$Alm$_6$Mj$_{16}$									
3.601(3)	0.00010(1)	298	296(4)	111(2)	92(1)	5.068(8)	9.07(3)	173(3)	92(1)
3.622(3)	1.00(6)	298	301(5)	111(5)	95(1)	5.11(1)	9.11(7)	174(5)	95(1)
3.664(3)	3.10(12)	298	314(7)	120(7)	97(1)	5.14(2)	9.26(9)	185(7)	97(1)
3.757(3)	7.9(6)	298	345(14)	138(14)	104(2)	5.25 (3)	9.58(19)	207(14)	104(2)
3.832(3)	12.1(7)	298	364(11)	150(11)	107(1)	5.28(1)	9.75(14)	222(11)	107(1)
3.874(3)	14.5(5)	298	374(7)	150(8)	112(2)	5.38(5)	9.84(8)	225(7)	112(2)
3.931(3)	18.0(4)	298	398(6)	168(5)	115(1)	5.40(1)	10.06(6)	245(5)	115(1)
3.981(3)	21.1(6)	298	412(7)	176(7)	118(1)	5.45(1)	10.18(7)	255(6)	118(1)
4.047(4)	26.0(1.6)	470	438(13)	195(12)	121(1)	5.47(1)	10.40(15)	276(13)	121(1)
4.022(4)	24.4(1.7)	470	435(9)	195(9)	120(2)	5.46(3)	10.40(17)	275(15)	120(2)
3.961(4)	20.4(1.9)	470	396(20)	170(20)	113(2)	5.34(4)	10.00(24)	245(20)	113(2)
3.897(4)	16.5(7)	470	389(9)	164(9)	113(1)	5.37(2)	9.99(11)	239(9)	113(1)
3.826(4)	12.4(1.3)	470	362(20)	151(20)	106(1)	5.25(3)	9.73(27)	221(20)	106(1)

with a Debye approximation that should describe thermal properties more reliably than the linear or polynomial moduli dependences often employed. In this formalism, the isothermal bulk modulus, K_T, is obtained as the second derivative of the Helmholtz free energy with respect to strain (f) and retains all terms that originate from the truncation to third order in strain of the free energy expansion:

$$K_T = (1 + 2f)^{5/2}$$
$$\times \left[K_0 + \left(3K_{T0}K'_{T0} - 5K_0\right)f + \frac{27}{2}\left(K_0K'_0 - 4K_0\right)f^2 \right]$$
$$+ (\gamma + 1 - q)\gamma \frac{\Delta E_{TH}(V, T)}{V}$$
$$- \frac{\gamma^2}{V} TC_V(V, T) - T_0 C_V(V, T_0) \right] \tag{9}$$

where

$$f = \frac{1}{2}\left[\left(\frac{V_0}{V}\right)^{2/3} - 1\right] = -\varepsilon \tag{10}$$

is the negative of the eulerian strain (ε), V is the molar volume, T is temperature, K_{T0} and K'_{T0} are the isothermal bulk modulus and its pressure derivative and the subscript zero indicates the reference state set at room conditions, $q = \left(\frac{\partial \ln \gamma}{\partial \ln V}\right)$ and γ is the Grüneisen parameter. ΔE_{TH} is the difference in the quasi-harmonic thermal energy between T and T_0 and C_V is the heat capacity at constant volume evaluated in the framework of Debye theory:

$$C_V = 9nN_A k_B \left(\frac{\theta}{T}\right)^{-3} \int_0^{\theta/T} \frac{x^4 e^x}{(e^x - 1)^2}dx \tag{11}$$

$$\theta = \theta_0 \left[1 + 6\gamma_0 f + \frac{1}{2}\left(-12\gamma_0 + 36\gamma_0^2 - 18\gamma_0 q_0\right)f^2\right]^{\frac{1}{2}} \tag{12}$$

where N_A is Avogadro's number and θ_0 is the room pressure value for the Debye temperature. The isothermal bulk modulus can be converted to the adiabatic bulk modulus K_s according to equation (8).

The shear modulus of an isotropic material can be calculated from the adiabatic elastic tensor according to the formulation of Stixrude and Lithgow-Bertelloni (2005):

$$G = (1 + 2f)^{5/2}\left[G_0 + \left(3K_0G'_0 - 5G_0\right)f\right.$$
$$+ \left(6K_0G'_0 - 24K_0 - 14G_0 + \frac{9}{2}K_0K'_0\right)f^2 \right]$$
$$- \eta_S \frac{\Delta E_{TH}(V, T)}{V} \tag{13}$$

where G_0 and G'_0 are the shear modulus and its pressure derivative at ambient conditions and η_S is the shear strain derivative of the Grüneisen parameter.

The formalism described above was used to fit the aggregate wave velocities V_P and V_S of Py$_{76}$Mj$_{24}$ and Py$_{78}$Alm$_6$Mj$_{16}$. The values of the EoS parameters (Table 3), K_{T0}, K'_{T0}, G_0, G'_0 and η_{S0} were obtained through a least square minimization of the differences between observed and calculated aggregate wave velocities. In the refinement the ambient volume V_0 was fixed to the value obtained from X-ray diffraction, the Grüneisen parameter γ_0 and the logarithmic volume derivative of the effective Debye temperature, q_0, were kept at values previously determined for garnets (Xu et al., 2008). The room pressure value of the Debye temperature was calculated from the experimental sound velocities according to the equations from Robie and Edwards (1966):

$$\theta_0 = \frac{h}{k}\left(3\frac{n}{4\pi V_0}\right)^{\frac{1}{3}}\left[3^{\frac{1}{3}}\left(\frac{1}{V_{P0}^3} + \frac{2}{V_{S0}^3}\right)^{-\frac{1}{3}}\right] \tag{14}$$

where h is the Plank constant, k is the Boltzmann constant, $n = 160$ is the number of atoms in the garnet unit cell, and V_{P0}
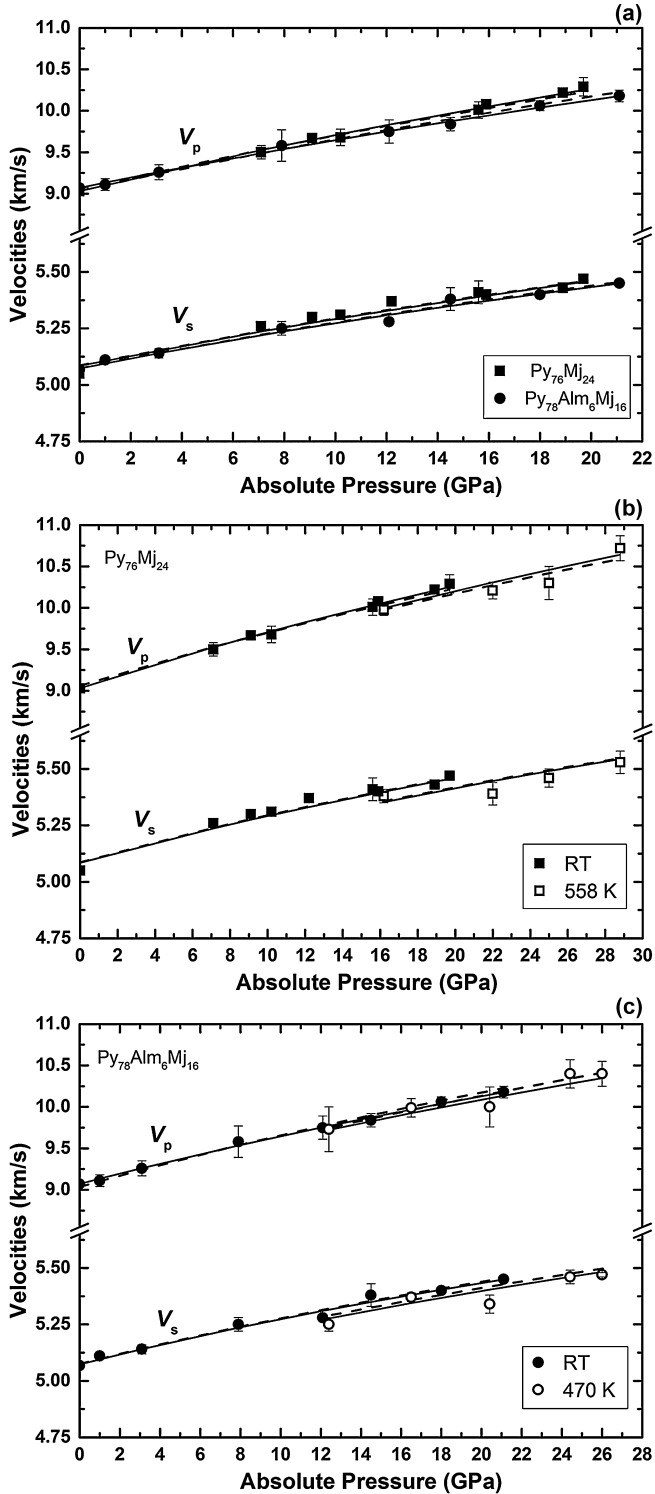
Fig. 2. Variation of the shear (V_s) and compressional (V_p) wave velocities as a function of absolute pressure of (a) $Py_{76}Mj_{24}$ and $Py_{78}Alm_6Mj_{16}$ at room temperature, (b) of $Py_{76}Mj_{24}$ at room temperature and at 558 K and (c) of $Py_{78}Alm_6Mj_{16}$ at room temperature and at 470 K. Solid curves are calculated from the parameters given in Table 3, whereas dashed curves are calculated from the thermo-elastic model parameters for garnet end members reported in Table 4.

and V_{S0} are the experimental longitudinal and transverse velocities at ambient conditions.

4. Discussion

4.1. Comparison with literature data

Fig. 3 shows determinations of the adiabatic bulk (K_{S0}) and shear (G_0) moduli for garnets along the Py–Mj join made in this and previous studies, plotted as a function of Mj content. The $Py_{78}Alm_6Mj_{16}$ sample is also plotted in addition to two other Alm and Alm and Gr bearing samples from Murakami et al. (2008) and Irifune et al. (2008) respectively. There seems to be a very good agreement between the several studies suggesting that G_0 decreases slightly with Mj content. Furthermore, $Py_{78}Alm_6Mj_{16}$ lies on the same trend, in excellent agreement with studies on the end-member Alm (Jiang et al., 2004), which has an almost identical G_0 to Py. The sample studied by Murakami et al. (2008) with 10% Alm plots slightly below the Py–Mj trend, on the other hand, although the difference is relatively small. The Alm and Gr bearing sample of Irifune et al. (2008) plots well above the trend, this is also consistent with measurements on the pure Gr end-member (Jiang et al., 2004), which shows a significantly greater G_0 (109 GPa) compared to Py. A little more scatter exists in the Py–Mj trend for K_{S0} with a number of relatively high estimates being made by ultrasonic studies at Mj contents ~40–50%. Many of the Brillouin scattering studies are in good agreement, however. That K_{S0} for $Py_{78}Alm_6Mj_{16}$ is higher than $Py_{76}Mj_{24}$ is in qualitative agreement with measurements made on pure Alm, which are higher than the Py end member (Jiang et al., 2004).

In Fig. 4 the moduli pressure derivatives K'_{S0} and G'_0 are plotted as a function of Mj content. There is very little variation in G'_0 even for Alm and Gr bearing samples but K'_{S0} covers a significant range with many ultrasonic measurements indicating relatively high values. As it can be seen in Fig. 2(a) there are clearly resolvable differences in the pressure derivatives between the $Py_{76}Mj_{24}$ and $Py_{78}Alm_6Mj_{16}$ samples. The combination of absolute pressure determinations and the use of a Ne pressure medium should ensure that these derivatives are of the highest precision measured for garnet samples to date. The lower values of K'_{S0} determined for the Alm bearing sample is consistent with the studies of Murakami et al. (2008) and Irifune et al. (2008).

Using the equation of state parameters obtained for $Py_{76}Mj_{24}$ and $Py_{76}Alm_8Mj_{16}$ (Table 3) sound velocities for these two compositions have been calculated at 20 GPa as a function of temperature up to 2000 K (Fig. 5). These are compared with the trend determined for a polycrystalline $Py_{23}Alm_6Mj_{50}Gr_{21}$ sample by Irifune et al. (2008) up to 1673 K and ~18 GPa.

Irifune et al. (2008) reported that the observed behavior was very different from that normally obtained by extrapolating linear dependences of elastic moduli with temperature, as commonly performed in literature studies (see for example Lu et al., 2013). Note, however, that the thermo-elastic model for the for $Py_{76}Mj_{24}$ and $Py_{76}Alm_8Mj_{16}$ samples reproduces the non-linear temperature behavior of the velocities.

4.2. Calculation of elastic properties for majoritic garnets from end member compositions

Garnet compositions are likely to vary within the upper mantle and transition zone as a result of pressure and temperature dependent changes in chemical partitioning between coexisting minerals in addition to variations in the mantle's bulk composition. In order to model the effects of these changes in chemistry on seismic velocities, elastic properties for complex garnet compositions need to be calculated from those of the major end-members, i.e. Py,

Table 3
EoS parameters of majoritic garnets.

| Sample	V_0 (cm^3 mol^{-1})	K_{s0} (GPa)	K_{T0} (GPa)	K'_{T0}	θ_0 (K)[a]	γ_0[b]	q_0[b]	G_0 (GPa)	G'_0	η_{s0}
Mg$_{3.24}$Al$_{1.53}$Si$_{3.23}$O$_{12}$ (Py$_{76}$Mj$_{24}$)	113.4	167(2)	166(2)	4.7(2)	791	1	1.4	91.8(7)	1.40(5)	1.3
Mg$_{3.01}$Fe$_{0.17}$Al$_{1.68}$Si$_{3.15}$O$_{12}$ (Py$_{78}$Alm$_6$Mj$_{16}$)	113.4	173(1)	172(1)	4.1(1)	795	1.06	1.4	92.7(6)	1.37(5)	1.9

[a] Calculated via equation (14).
[b] Fixed to previously determined values (Xu et al., 2008).

Table 4
Thermo-elastic parameters of mantle components used for calculating the sound wave velocities and densities as a function of pressure and temperature in the transition zone.

Phase	Formula	V_0 (cm^3/mol)	K_{T0} (GPa)	K'_{T0}	θ_0 (K)	γ_0	q_0	G_0 (GPa)	G'_0	η_{s0}
Pyrope	Mg$_3$Al$_2$Si$_3$O$_{12}$	*113.08*	*171*	**4.3**	**804**[a]	*1.01*	*1.4*	*94*	*1.4*	**1.2**
Majorite	Mg$_4$Si$_4$O$_{12}$	**113.97**	**160**	**5.0**	**779**[a]	*0.98*	*1.5*	**86**	*1.4*	**1.4**
Almandine	Fe$_3$Al$_2$Si$_3$O$_{12}$	*115.43*	**175**	**3.7**	*741*	*1.06*	*1.4*	*96*	**1.1**	*2.1*
Grossular	Ca$_3$Al$_2$Si$_3$O$_{12}$	*125.12*	*167*	*3.9*	*823*	*1.05*	*1.9*	*109*	*1.2*	*2.4*
Wadsleyite	Mg$_2$SiO$_4$	*40.52*	*169*	*4.3*	*853*	*1.21*	*2*	*112*	*1.4*	*2.6*
Wadsleyite	Fe$_2$SiO$_4$	*42.80*	*169*	*4.3*	*719*	*1.21*	*2*	*72*	*1.4*	*1.1*
Ringwoodite	Mg$_2$SiO$_4$	*39.49*	*185*	*4.2*	*891*	*1.11*	*2.4*	*123*	*1.4*	*2.3*
Ringwoodite	Fe$_2$SiO$_4$	*41.86*	*213*	*4.2*	*652*	*1.26*	*2.4*	*92*	*1.4*	*1.8*
Ca-Perovskite	CaSiO$_3$	*27.45*	*236*	*3.9*	*802*	*1.89*	*0.9*	*157*	*2.2*	*1.3*
Stishovite	SiO$_2$	*14.02*	*314*	*3.8*	*1055*	*1.35*	*2.9*	*220*	*1.9*	*4.6*

[a] Calculated via equation (14); values in italics are taken from Xu et al. (2008) and are in good agreement with recent experimental measurements, whereas values that differ from those reported in the compilation of Xu et al. (2008) are reported in bold.
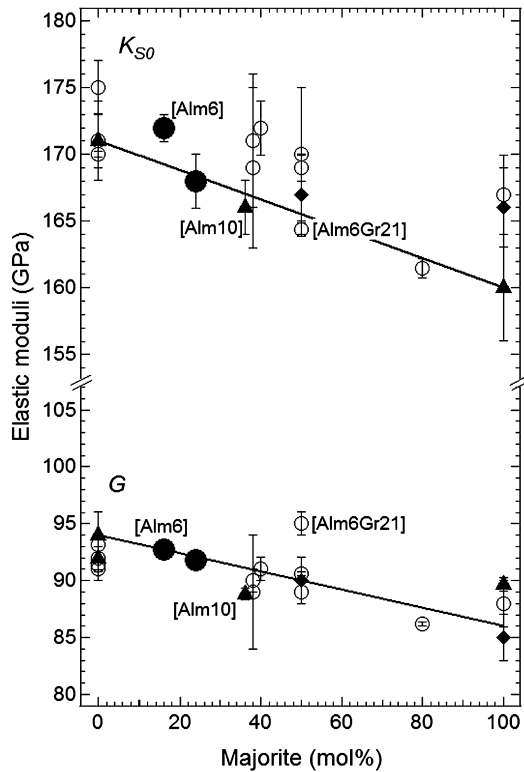
Fig. 3. Ambient elastic moduli (K_{S0} and G_0) as a function of majorite content along the binary majorite–pyrope join. Filled circles: this study; open circles: ultrasonic measurements from Ridgen et al. (1994), Chen et al. (1999), Liu et al. (2000), Gwanmesia et al. (1998, 2006, 2009), Irifune et al. (2008), Zhou et al. (2012), Liu et al. (2015); filled triangles and diamonds: Brillouin spectroscopy measurements on single-crystal and polycrystalline samples, respectively, by Pacalo and Weidner (1997), Sinogeikin and Bass (2000, 2002), Murakami et al. (2008). Three measurements made on more complex compositions have the proportions of almandine [Alm] and grossular [Gr] in the garnets indicated. The solid lines show a linear dependence of K_{S0} and G_0 with composition calculated using the end-member data reported in Table 4.
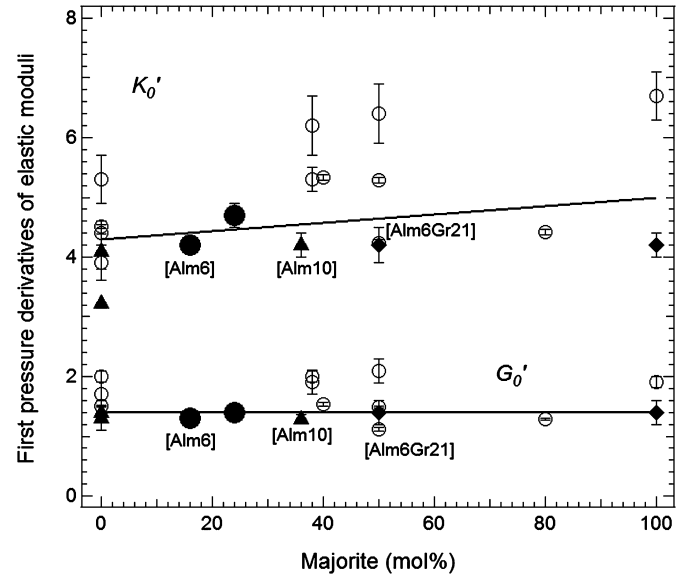

Fig. 4. Ambient first pressure derivatives of the elastic moduli (K'_0 and G'_0) as a function of majorite content along the binary majorite–pyrope system. Symbols are the same as in Fig. 3. The solid lines show a linear dependence of K'_0 and G'_0 with composition calculated using the end-member data reported in Table 4.

Mj, Alm and Gr. The elastic properties of a phase consisting of a solid solution of n end-members in a single mineral phase can be derived through a weighted summation of the individual elastic properties of the corresponding end-members:

$$\psi_{ss} = \frac{1}{\sum_{i=1}^{n} \frac{1}{m_i V_i} \sum_{i=1}^{n} \frac{m_i V_i}{\psi_i}} \tag{15}$$

where ψ_{ss} is the bulk elastic property of interest, ψ_i is the elastic property of component i and V_i and m_i are the volume and mole fraction of component i. This summation assumes that the property in question varies as a linear function of the end-member properties. Recent determinations of K'_{T0} for solid solutions along
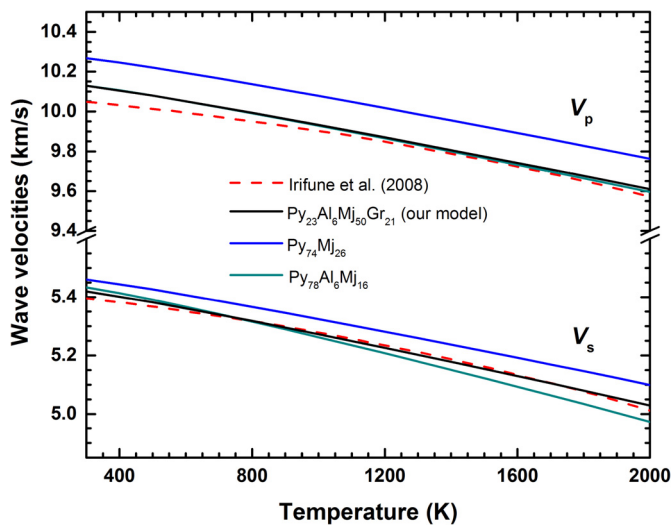
Fig. 5. The variation in acoustic velocities of $Py_{76}Mj_{24}$ (blue) and $Py_{76}Alm_8Mj_{16}$ (green) at 20 GPa, extrapolated as a function of temperature using the EoS parameters reported in Table 3. The velocities of a complex garnet composition, $Py_{23}Alm_6Mj_{50}Gr_{21}$ (black), have been calculated using an end-member model based on the experimental data (Table 4). The dashed curves (red) show fits to ultrasonic measurements performed on a similar $Py_{23}Alm_6Mj_{50}Gr_{21}$ garnet composition by Irifune et al. (2008).

the Gr–Py binary suggest that this may not always be an accurate assumption (Du et al., 2015). Due to potential non-linear effects it is possible that fictive end-member properties, determined using data on garnets that have intermediate compositions (and that may, therefore, be closer to those in the mantle), may reproduce the experimental velocities better than using data obtained for end-member compositions.

Using the equation of state model described in Section 3.3, velocities for the $Py_{76}Mj_{24}$ and $Py_{78}Alm_6Mj_{16}$ samples were calculated through a summation of the elastic properties of the appropriate end-members, as in equation (15). The initial values of V_0, K'_{T0}, θ_0, γ_0, q_0, G_0, G'_0, and η_{S0} for the Py, Mj and Alm end-members were initially taken from Xu et al. (2008) (Table 4), although Debye temperatures for Py and Mj were recalculated in accordance with equation (14). The resulting velocities were then compared with the high pressure and temperature experimental values, and the properties for Py, Mj and Alm were refined to minimize the calculated and observed differences. Values which differ from those reported in the compilation of Xu et al. (2008) are reported in bold in Table 4. The lines in Figs. 3 and 4 show how the moduli and their derivatives change across the Py–Mj join according to the resulting model.

Using data for Gr from the literature (Xu et al., 2008), the model has been used to calculate acoustic velocities for the $Py_{23}Alm_6Mj_{50}Gr_{21}$ composition examined by Irifune et al. (2008). The model calculations, performed at 20 GPa as a function of temperature, are compared with the experimental curves of Irifune et al. (2008) in Fig. 5. The shear velocity curve reported by Irifune et al. (2008) is extremely well reproduced by the resulting model, both in terms of the absolute values and the velocity gradient with temperature. The calculated longitudinal velocities are higher by $\sim$1 km s^{-1} than the experimental values at room temperature but converge to be in excellent agreement at mantle temperatures. Although the agreement should be in principal good at all temperatures, it is possible that in the multianvil measurements deviatoric stresses at low temperatures cause this difference, which decreases with temperature (Gwamnesia et al., 2006).

4.3. Implication for the Earth's transition zone

The elastic properties of garnets determined in this study were used along with additional literature data (summarized in Table 4) to calculate seismic velocities for pyrolite, harzburgite and MORB bulk compositions at the base of the transition zone, in the depth range between 480 and 660 km. Calculations were not performed at lower pressures due to the absence of sufficient data on the clinopyroxene mineral properties. The calculations were performed along an adiabat with a potential temperature of 1673 K employing thermodynamic models to describe variations in the proportion and chemistry of the mineral phases. A Voigt–Reuss–Hill averaging scheme was used to extract the aggregate elastic properties from those of the individual minerals. Phase relations at the base of the transition zone are relatively simple and can be described using models that have been derived within a number of experimental studies (Frost, 2003; Frost and Doleîs, 2007; Saikia et al., 2008).

At 480 km a pyrolite composition will be comprised of only wadsleyite and majoritic garnet (Irifune and Isshiki, 1998). Based on the bulk composition and using Fe–Mg partitioning data from Irifune and Isshiki (1998) it is then straight forward to calculate the compositions of both phases, which results in 42 vol.% garnet with the composition $Py_{14}Alm_8Mj_{56}Gr_{21}$. At approximately 540 km, wadsleyite undergoes a phase transition to ringwoodite over a depth interval of approximately 20 km, which can be described using thermodynamic models that have been fit to experimental data (Frost, 2003; Frost and Doleîs, 2007). Between 480 and 620 km the garnet composition and proportion remain constant apart from small changes in Fe–Mg partitioning between wadsleyite and ringwoodite. However, at 620 km $CaSiO_3$ perovskite (Ca-Pv) starts to exsolve from garnet, with the volume proportion of Ca-Pv gradually increasing with depth at the expense of the grossular component of garnet (Saikia et al., 2008). As a consequence, the garnet composition loses Ca but also becomes less majoritic. The gradual increase of Ca-Pv and the consequent compositional variations in garnet can be described using the thermodynamic model of Saikia et al. (2008). At the base of the transition zone the pyrolite mineralogy comprises 58 vol.% ringwoodite, $(Mg_{0.9}Fe_{0.1})_2SiO_4$, 36 vol.% garnet ($Py_{34}Alm_9Mj_{51}Gr_4$) and 6 vol% $CaSiO_3$ perovskite.

In contrast to pyrolite, an average MORB composition in the mantle transition zone is composed almost entirely of garnet (89 vol.%) with additional stishovite (11 vol.%) (Irifune et al., 1986). As for the pyrolite composition, in the lower transition zone Ca-Pv starts to exsolve from majoritic garnet, the phase relations of which can also be described using the thermodynamic model of Saikia et al. (2008). Because the Ca content of subducted oceanic crust (MORB) is higher than that of pyrolite, garnets should become saturated in $CaSiO_3$ at lower pressures. However, the saturation pressure is also a function of the garnet majorite component (Saikia et al., 2008), which is lower in MORB with respect to a pyrolite composition. These two effects act in opposite directions and ensure that the exsolution of $CaSiO_3$ perovskite from garnet occurs at approximately the same depth as observed for the pyrolite composition. With increasing pressure, as $CaSiO_3$ perovskite exsolves, the garnet becomes more Al-rich. At the base of the transition zone the MORB mineralogy comprises 72 vol.% garnet ($Py_{58}Alm_{20}Mj_3Gr_{19}$), 11 vol, % SiO_2 and 17 vol.% $CaSiO_3$ perovskite.

Harzburgite phase relations are similar to those of pyrolite over the same depth interval, with the main difference being a higher proportion of $(Fe,Mg)_2SiO_4$. At 480 km the average harzburgite composition employed (Irifune and Ringwood, 1987b) is calculated to comprise 81.5 vol.% wadsleyite and 18.5 vol.% of majoritic garnet with the composition $Alm_{12}Mj_{80}Gr_8$. Phase transformations are similar to those in pyrolite, although due to the low Ca content the exsolution of $CaSiO_3$ is almost insignificant and the low Al content results in a more majorite rich garnet.
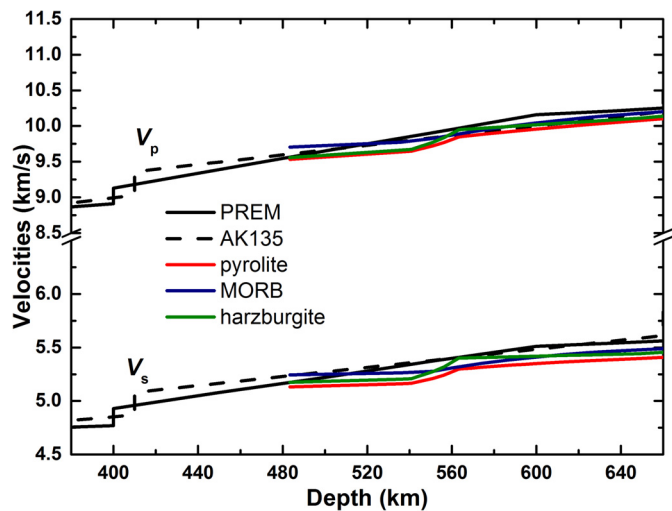
Fig. 6. Sound velocities for pyrolite (red) harzburgite (green) and MORB (blue) compositions obtained from the parameters reported in Table 4 along a mantle adiabat of 1673 K at pressures corresponding to the transition zone. The solid and dashed black curves show PREM and AK135 seismic reference models, respectively. Voigt and Reuss bounds for each lithology can be found in Fig. S4 in the supplementary information.

The sound velocities V_S and V_P calculated for the three bulk compositions described above are compared with the seismic reference models PREM and AK135 in Fig. 6.

Although the pyrolite model is in agreement at least with AK135 in terms of V_P, there is a consistent negative deviation for V_S, by ∼0.2 km/s, between pyrolite and both reference models over the 150 km of the base of the transition zone. Garnet elastic properties are the main reason for this deviation as both ringwoodite and CaSiO$_3$-perovskite have velocities that are above both reference models at these conditions. Reference models are globally averaged velocity structures and it should, in principal, be possible to approximate this structure using an average mantle composition, mineralogy and temperature. Reference models are unlikely to capture the detail of the velocity structure, however, particularly in the transition zone, due to the overly simplified polynomial functions upon which they are based (Cammarano et al., 2005). Trade-offs between the magnitude of seismic discontinuities and the velocity gradient, for example, are likely to cause inaccuracies in the determinations of both. On average, however, negative deviations from the real mantle velocity structure would be expected to be balanced by near-by positive deviations. This would appear not to be the case in the transition zone, however, if a pyrolite model along a 1600 K adiabat is assumed to resemble the real mantle.

Irifune et al. (2008) also reported that estimated velocities for pyrolite are lower than the reference models at approximately 575 km, but suggested that the subsequent exsolution of CaSiO$_3$ perovskite from garnet would decrease the discrepancy towards the base of the transition zone. Sinogeikin and Bass (2002) similarly argued that CaSiO$_3$ perovskite exsolution would raise the velocity gradient. Note, however, that in this study, the gradual formation of CaSiO$_3$-rich perovskite and the resulting compositional variations in garnet have been taken into account. A very slight increase in the velocity gradient for the pyrolite model occurs above 570 km due to CaSiO$_3$ exsolution. Without this exsolution the pyrolite velocities would have the same gradient as the harzburgite model. Although shear wave properties of CaSiO$_3$ perovskite are poorly constrained, the G_0 used in the current model (Xu et al., 2008) is at the very high limit of recent theoretical studies (Kawai and Tsuchiya, 2015) and is higher than experimental estimates (Kudo et al., 2012). Therefore, it seems unlikely that the V_S for

CaSiO$_3$ perovskite is significantly underestimated, in fact the contrary seems more likely. It appears, therefore, that pyrolite along a 1673 K adiabat provides a poor match to seismic reference models at the base of the transition zone.

Other bulk compositions have been proposed for the transition zone, such as piclogite (Bass and Anderson, 1984; Anderson and Bass, 1986), however from Fig. 6 it appears that increasing the basaltic component of a mineralogical assemblage does not result in an increase of V_S values to levels compatible with the reference models. For the MORB composition, the exsolution of CaSiO$_3$ perovskite can be clearly seen to cause an increase in gradient above 550 km. Although the resulting gradient is closer to the reference models, the absolute values remain 0.1 km/s below both reference models throughout the base of the transition zone.

A number of other effects that could, in principal, cause differences between mineral and seismic models are also likely to further lower the calculated mineral velocities. For example, anelastic effects that cause dispersion and variations of mineral velocities as a function of acoustic wavelength are likely to lower the velocities of mineral models that account for them. Similarly, the presence of minor defects such as those caused by the presence of dissolved OH$^-$ in minerals also will only lower velocities (Jacobsen, 2006).

If subducted material accumulates at the base of the transition zone it is possible that a significant portion of the material in this regions is composed of melt depleted harzbugite. As shown in Fig. 6, although melt depletion increases the proportion of (Fe, Mg)$_2$SiO$_4$ phase which raises velocities, they still fall below the reference models.

One of the few remaining plausible explanations for the deviation between mineral and seismic models at the base of the transition zone would be if the average mantle temperature over this depth interval is below the 1673 K adiabat. While mantle adiabatic temperatures determined from erupted basalt melt compositions vary by approximately ±150°, (Lee et al., 2009), the estimated temperature needed for the pyrolite model to match the seismic model at the base of the transition zone is ∼500 K lower than 1673 K. This would place mantle temperatures far outside of the range of adiabatic temperature estimates from the surface or from temperature estimates based on the depth of the 410 km discontinuity (Frost, 2008). Saikia et al. (2008) noted that to associate the 520 km seismic discontinuity with the wadsleyite to ringwoodite transformation requires lower than expected average mantle temperatures. This can be seen in Fig. 6, where the wadsleyite to ringwoodite transformation along a 1673 K adiabat occurs at 550 km, and only if temperatures were ∼300 K lower would the transition occur at 520 km. Saikia et al. (2008) suggested that a possible cause of lower mantle temperatures may be the presence of subducting slabs stagnating at the base of the transition zone and flattening out to form significant lateral cold heterogeneities. Some tomographic models (e.g. Kárason and Van der Hilst, 2000) appear to clearly indicate that such heterogeneities exist. As temperatures in the center of such slabs could be easily 600 K below the average mantle, they could drag down average mantle temperatures at these depths, assuming that the lateral anomalies were large enough. Furthermore it is possible that a significant proportion of this material will be of near harzburgite composition. It can be estimated that temperatures would have to be only 200 K below the 1673 K adiabat for harzburgite mineral model velocities to match seismic reference models at the base of the transition zone. If such global horizontal anomalies exist, this average reduction in temperature may be plausible and would be also consistent with the 520 km seismic discontinuity being caused by the wadsleyite to ringwoodite transformation.

A further issue that needs to be investigated is the effect of the mineral akimotoite which is expected to form in both harzburgite and pyrolite compositions if temperatures at the base of the transition zone were several hundred degrees lower than the 1673 K adiabat. The elastic properties of akimotoite are poorly explored, however in a recent experimental study the presence of akimotoite has been proposed to raise seismic velocities at the base of the transition zone (Zhou et al., 2014).

Acknowledgements

Appendix A. Supplementary material

Supplementary material related to this article can be found online at http://dx.doi.org/10.1016/j.epsl.2016.07.019.

References

Ahrens, T.J., 1995. Mineral Physics and Crystallography, A Handbook of Physical Constants. AGU Publications, Washington, DC, pp. 64–97.

Anderson, D.L., Bass, J.D., 1986. Transition region of the Earth's upper mantle. Nature 320, 321–328. http://dx.doi.org/10.1038/320321a0.

Angel, R.J., Finger, L.W., 2011. SINGLE: a program to control single-crystal diffractometers. J. Appl. Crystallogr. 44, 247–251. http://dx.doi.org/10.1107/S0021889810042305.

Angel, R.J., Finger, L.W., Hazen, R.M., Kanzaki, M., Weidner, D.J., Liebermann, R.C., Veblen, D.R., 1989. Structure and twinning of single-crystal $MgSiO_3$ garnet synthesised at 17 GPa and 1800 °C. Am. Mineral. 74, 509–512.

Bass, J.D., Anderson, D.L., 1984. Composition of the upper mantle-geophysical tests of two petrological models. Geophys. Res. Lett. 11, 237–240. http://dx.doi.org/10.1029/GL011i003p00229.

Bass, J.D., Kanzaki, M., 1990. Elasticity of a majorite–pyrope solid solution. Geophys. Res. Lett. 17. http://dx.doi.org/10.1029/GL017i011p01989.

Cammarano, F., Deuss, A., Goes, S., Giardini, D., 2005. One-dimensional physical reference models for the upper mantle and transition zone: combining seismic and mineral physics constraints. J. Geophys. Res. 110, B01306. http://dx.doi.org/10.1029/2004JB003272.

Chen, G., Cooke, J.A., Gwanmesia, G.D., Liebermann, R.C., 1999. Elastic wave velocities of $Mg_3Al_2Si_3O_{12}$–pyrope garnet to 10 GPa. Am. Mineral. 84, 384–388.

Conrad, P.G., Zha, C.-S., Mao, H.-K., Hemley, R.J., 1999. The high-pressure, single crystal elasticity of pyrope, grossular and andradite. Am. Mineral. 84, 374–383.

Du, W., Clark, S.M., Walker, D., 2015. Thermo-compression of pyrope–grossular garnet solid solutions: non-linear compositional dependence. Am. Mineral. 100, 215–222. http://dx.doi.org/10.2138/am-2015-4752.

Frost, D.J., 2003. The structure and sharpness of $(Mg, Fe)_2SiO_4$ phase transformations in the transition zone. Earth Planet. Sci. Lett. 216, 313–318. http://dx.doi.org/10.1016/S0012-821X(03)00533-8.

Frost, D.J., 2008. The upper mantle and transition zone. Elements 4 (3), 171–176. http://dx.doi.org/10.2113/GSELEMENTS.4.3.171.

Frost, D.J., Dolejš, D., 2007. Experimental determination of the effect of H_2O on the 410 km discontinuity. Earth Planet. Sci. Lett. 256 (1–2), 182–195. http://dx.doi.org/10.1016/j.epsl.2007.01.023.

Gwanmesia, G.D., Chen, G., Liebermann, R.C., 1998. Sound velocities in $MgSiO_3$-garnet to 9 GPa at room temperature. Geophys. Res. Lett. 25, 4553–4556. http://dx.doi.org/10.1029/1998GL900189.

Gwanmesia, G.D., Zhang, J., Darling, K., Kung, J., Li, B., Wang, L., Neuville, D., Liebermann, R.C., 2006. Elasticity of polycrystalline pyrope ($Mg_3Al_2Si_3O_{12}$) to 9 GPa and 1000 °C. Phys. Earth Planet. Inter. 155, 179–190. http://dx.doi.org/10.1016/j.pepi.2005.10.008.

Gwanmesia, G.D., Wang, L., Triplett, R., Liebermann, R.C., 2009. Pressure and temperature dependence of the elasticity of pyrope–majorite [$Py_{60}Mj_{40}$ and $Py_{50}Mj_{50}$] garnets solid solution measured by ultrasonic interferometry technique. Phys. Earth Planet. Inter. 174, 105–112. http://dx.doi.org/10.1016/j.pepi.2008.07.029.

Irifune, T., Ringwood, A.E., 1987a. Phase transformations in primitive MORB and pyrolite compositions to 25 GPa and some geophysical implications. In: Manghnani, M.H., Syono, Y. (Eds.), High Pressure Research in Mineral Physics. Terra Scientific, Tokyo, pp. 231–242.

Irifune, T., Ringwood, A.E., 1987b. Phase transformations in a harzburgite composition to 26 GPa: implications for dynamical behaviour of the subducting slab. Earth Planet. Sci. Lett. 86, 365–376. http://dx.doi.org/10.1016/0012-821X(87)90233-0.

Irifune, T., Isshiki, M., 1998. Iron partitioning in a pyrolite mantle and the nature of the 410-km seismic discontinuity. Nature 392, 702–705. http://dx.doi.org/10.1038/33663.

Irifune, T., Sekine, T., Ringwood, A.E., Hibberson, W.O., 1986. The eclogite–garnetite transformation at high pressure and some geophysical implications. Earth Planet. Sci. Lett. 77, 245–256.

Irifune, T., Higo, Y., Inoue, T., Kono, Y., Ohfuji, H., Funakoshi, K., 2008. Sound velocities of majorite garnet and the composition of the mantle transition region. Nature 451, 814–817. http://dx.doi.org/10.1038/nature06551.

Ita, J., Stixrude, L., 1992. Petrology, elasticity, and composition of the mantle transition zone. J. Geophys. Res. 97 (B5), 6849–6866. http://dx.doi.org/10.1029/92JB00068.

Jacobsen, S.D., 2006. Effect of water on the equation of state of nominally anhydrous minerals. In: Keppler, H., Smyth, J.R. (Eds.), Water in Nominally Anhydrous Minerals. In: Reviews in Mineralogy and Geochemistry, vol. 62. Geochemical Society Mineralogical Society of America, pp. 321–342.

Jiang, F.M., Speziale, S., Duffy, T.S., 2004. Single-crystal elasticity of grossular- and almandine-rich garnets to 11 GPa by Brillouin scattering. J. Geophys. Res. 109 (B10), B10210. http://dx.doi.org/10.1029/2004JB003081.

Kárason, H., Van der Hilst, R.D., 2000. Constraints on mantle convection from seismic tomography. In: Richards, M.R., Gordon, R.G., Van der Hilst, R.D. (Eds.), The History and Dynamics of Global Plate Motion. In: Geophys. Monog. Ser., vol. 121. AGU, Washington, D.C., pp. 277–288.

Kato, T., Kumazawa, M., 1985. Garnet phase of $MgSiO_3$ filling the pyroxene–ilmenite gap at very high temperature. Nature 316, 803–805. http://dx.doi.org/10.1038/316803a0.

Kawai, K., Tsuchiya, T., 2015. Small shear modulus of cubic $CaSiO_3$ perovskite. Geophys. Res. Lett. 42, 2718–2726. http://dx.doi.org/10.1002/2015GL063446.

Keppler, H., Frost, D.J., 2005. Introduction to minerals under extreme conditions. In: Miletich, R. (Ed.), Mineral Behaviour at Extreme Conditions. In: EMU Notes in Mineralogy, vol. 7, pp. 1–30.

King, H.E., Finger, L., 1979. Diffracted beam crystal centering and its application to high pressure crystallography. J. Appl. Crystallogr. 12, 374–378. http://dx.doi.org/10.1107/S0021889879012723.

Kudo, Y., Hirose, K., Murakami, M., Asahara, Y., Ozawa, H., Ohishi, Y., Hirao, N., 2012. Sound velocities measurements of $CaSiO_3$ perovskite to 133 GPa and implications for lowermost mantle seismic anomalies. Earth Planet. Sci. Lett. 1–7, 349–350. http://dx.doi.org/10.1016/j.epsl.2012.06.040.

Kurnosov, A., Kantor, I., Boffa Ballaran, T., Lindhardt, S., Dubrovinsky, L., Kuznetsov, A., Zehnder, B.H., 2008. A novel gas-loading system for mechanically closing of various types of diamond anvil cells. Rev. Sci. Instrum. 79, 045110. http://dx.doi.org/10.1163/1.2902506.

Lee, C.T.A., Luffi, P., Plank, T., Dalton, H.A., Leeman, W.P., 2009. Constraints on the depths and temperatures of basaltic magma generation on Earth and other terrestrial planets. Earth Planet. Sci. Lett. 279, 20–33. http://dx.doi.org/10.1016/j.epsl.2008.12.020.

Liu, J., Chen, G., Gwanmesia, G.D., Liebermann, R.C., 2000. Elastic wave velocities of pyrope–majorite garnets ($Py_{62}Mj_{38}$ and $Py_{50}Mj_{50}$) to 9 GPa. Phys. Earth Planet. Inter. 120, 153–163. http://dx.doi.org/10.1016/S0031-9201(00)00152-7.

Liu, Z., Irifune, T., Gréaux, S., Arimoto, T., Shinmei, T., Higo, Y., 2015. Elastic wave velocity of polycrystalline $Mj_{80}Py_{20}$ garnet to 21 GPa and 2000 K. Phys. Chem. Miner. 42, 213–222. http://dx.doi.org/10.1007/s00269-014-0712-y.

Lu, C., Mao, Z., Lin, J.-F., Zhuravlev, K.K., Tkachev, S.N., Prakapenka, V.B., 2013. Elasticity of single-crystal iron-bearing pyrope up to 20 GPa and 750 K. Earth Planet. Sci. Lett. 361, 134–142. http://dx.doi.org/10.1016/j.epsl.2012.11.041.

Murakami, M., Sinogeikin, S.V., Litasov, K., Ohtani, E., Bass, J.D., 2008. Single-crystal elasticity of iron-bearing majorite to 26 GPa: implications for seismic velocity structure of the mantle transition zone. Earth Planet. Sci. Lett. 274, 339–345. http://dx.doi.org/10.1016/j.epsl.2008.07.045.

O'Neill, B., Bass, J.D., Rossman, G.R., Geiger, C.A., Langer, K., 1991. Elastic properties of pyrope. Phys. Chem. Miner. 17, 617–621. http://dx.doi.org/10.1007/BF00203841.

Pacalo, R.E.G., Weidner, D.J., 1997. Elasticity of majorite, $MgSiO_3$ tetragonal garnet. Phys. Earth Planet. Inter. 99, 145–154. http://dx.doi.org/10.1016/S0031-9201(96)03158-5.

Paterson, M.S., 1982. The determination of hydroxyl by infrared absorption in quartz, silicate glasses and similar materials. Bull. Minéral. 105, 20–29.

Rekhi, S., Dubrovinsky, L., Saxena, S.K., 1999. Temperature-induced ruby fluorescence shifts up to a pressure of 15 GPa in an externally heated diamond anvil cell. High Temp.- High Pressures 31, 299–305. http://dx.doi.org/10.1068/htrt161.

Rigden, S.M., Gwanmesia, G.D., Liebermann, R.C., 1994. Elastic wave velocities of a pyrope–majorite garnet to 3 GPa. Phys. Earth Planet. Inter. 86, 35–44. http://dx.doi.org/10.1016/0031-9201(94)05060-0.

Ringwood, A.E., 1967. Pyroxene–garnet transition in the Earth's mantle. Earth Planet. Sci. Lett. 2, 255–263.

Rivers, M., Prakapenka, V.B., Kubo, A., Pullins, C., Holl, C.M., Jacobsen, S.D., 2008. The COMPRES/GSECARS gas-loading system for diamond anvil cells at the Advanced Photon Source. High Press. Res. 28 (3), 273–292. http://dx.doi.org/10.1080/08957950802333593.

Robie, R.A., Edwards, J.L., 1966. Some Debye temperatures from single crystal elastic constant data. J. Appl. Phys. 37, 2659–2663. http://dx.doi.org/10.1063/1.1782100.

Saikia, A., Frost, D.J., Rubie, D.C., 2008. Splitting of the 520-kilometer seismic discontinuity and chemical heterogeneity in the mantle. Science 319 (5869), 1515–1518. http://dx.doi.org/10.1126/science.1152818.

Sinogeikin, S.V., Bass, J.D., 2000. Single-crystal elasticity of pyrope and MgO to 20 GPa by Brillouin scattering in the diamond anvil cell. Phys. Earth Planet. Inter. 120, 43–62. http://dx.doi.org/10.1016/S0031-9201(00)00143-6.

Sinogeikin, S.V., Bass, J.D., 2002. Elasticity of majorite and a majorite–pyrope solid solution to high pressure: implications for the transition zone. Geophys. Res. Lett. 29 (2), 1017. http://dx.doi.org/10.1029/2001GL013937.

Stixrude, L., Lithgow-Bertelloni, C., 2005. Thermodynamics of mantle minerals, I: physical properties. Geophys. J. Int. 162, 610–632. http://dx.doi.org/10.1111/j.1365-246X.2005.02642.x.

Trots, D.M., Kurnosov, A., Boffa Ballaran, T., Tkachev, S., Zhuravlev, K., Prakapenka, V., Berkowski, M., Frost, D.J., 2013. The Sm: YAG primary fluorescence pressure scale. J. Geophys. Res., Solid Earth 118. http://dx.doi.org/10.1002/2013JB010519.

Wang, Z., Ji, S., 2001. Elasticity of six polycrystalline silicate garnets at pressure up to 3.0 GPa. Am. Mineral. 86, 1209–1218. http://dx.doi.org/10.2138/am-2001-1009.

Whitfield, C.H., Brody, E.M., Bassett, W.A., 1976. Elastic moduli of NaCl by Brillouin scattering at high pressure in a diamond anvil cell. Rev. Sci. Instrum. 47, 942. http://dx.doi.org/10.1063/1.1134778.

Xu, W., Lithgow-Bertelloni, C., Stixrude, L., Ritsema, J., 2008. The effect of bulk composition and temperature on mantle seismic structure. Earth Planet. Sci. Lett. 275, 70–79. http://dx.doi.org/10.1016/j.epsl.2008.08.012.

Zhou, C., Irifune, T., Gréaux, S., Whitaker, M.L., Shinmei, T., Ohfuji, H., Negishi, R., Higo, Y., 2012. Elasticity and sound velocities of polycrystalline $Mg_3Al_2(SiO_4)_3$ garnet up to 20 GPa and 1700 K. J. Appl. Phys. 112, 014910. http://dx.doi.org/10.1063/1.4736407.

Zhou, C., Gréaux, S., Nishiyama, N., Irifune, T., Higo, Y., 2014. Sound velocities measurement on $MgSiO_3$ akimotoite at high pressures and high temperatures with simultaneous in situ X-ray diffraction and ultrasonic study. Phys. Earth Planet. Inter. 228, 97–105. http://dx.doi.org/10.1016/j.pepi.2013.06.005.